Molecular Vision 2021; 27:403-414 <http://www.molvis.org/molvis/v27/403>
Received 25 January 2020 | Accepted 29 June 2021 | Published 1 July 2021

Functional analysis of deleterious *EPHA2* SNPs in lens epithelial cells

Dan Li,[1,4] Xiaoyan Han,[1,4] Zhennan Zhao,[1,4] Yi Lu,[1,4] Jin Yang[1,4]

(The first three authors contributed equally to this work.)

[1]Eye Institute, Eye & ENT Hospital of Fudan University, Shanghai, China; [2]Shanghai Key Laboratory of Visual Impairment and Restoration, Shanghai, China; [3]NHC Key Laboratory of Myopia, Fudan University, Fudan China; [4]Laboratory of Myopia, Chinese Academy of Medical Sciences, Shanghai, China

Purpose: Ephrin (Eph) receptor A2 (*EPHA2*) polymorphism has been associated with age-related cataract (ARC) in different populations worldwide, but the mechanisms by which this polymorphism results in the development of ARC are unclear. Here, we chose four *EPHA2* single nucleotide polymorphisms (SNPs; rs35903225, rs145592908, rs137853199, and rs116506614) and studied their function in human lens epithelial cells (LECs).

Methods: The four *EPHA2* mutants were overexpressed using lentiviral transduction in human LECs. Cells expressing wild-type (WT) and mutated EPHA2 were subjected to quantitative PCR (qPCR), western blot, immunoprecipitation (IP), and transwell migration assay. MG132 and chloroquine were used to inhibit the degradation of the WT and mutated EPHA2. The structural changes induced by rs137853199 were predicted and optimized using Schrödinger software. IP–mass spectrometry (IP-MS) was performed to examine the proteins that directly interact with WT and rs137853199 EPHA2. Sanger sequencing was performed to determine the frequency of rs137853199 in 184 patients with ARC (73 cortical cataracts, 56 nuclear cataracts, and 55 posterior subcapsular cataracts) and 49 normal controls.

Results: Compared with the WT and the other three mutations, the rs137853199 mutation specifically resulted in a significant decrease in the expression of EPHA2. We identified that EPHA2 rs137853199 is degraded via the ubiquitin–proteasomal pathway through a lysine-48 (K48) residue linkage. Furthermore, the knockdown of *EPHA2* reduced cell migration; while the overexpression of WT *EPHA2* rescued this defect, the overexpression of rs137853199 *EPHA2* did not. In addition, in cells overexpressing rs137853199 *EPHA2*, the expression of β-catenin, a key protein that regulates cell migration, significantly decreased. We predicted that rs137853199 would induce a conformational change at a linker position in the carboxyl terminal of EPHA2. The IP-MS results showed that the main molecular functions of the proteins that specifically bind WT or rs137853199 EPHA2 are binding and catalysis, while the main protein class is the protein-modifying enzyme. Finally, we discovered that the minor allele frequency of rs137853199 was significantly higher in cortical cataract patients than it was in normal controls.

Conclusions: In summary, these findings suggest a mechanism by which a point mutation in *EPHA2* disrupts protein stability, expedites protein degradation, and decreases cell mobility. Importantly, this mutant is associated with cortical cataracts.

Cataract is a leading cause of blindness globally, and surgery is the only effective treatment. According to the World Health Organization, cataract accounts for 51% of world blindness, and the associated surgery costs pose a great economic burden to society. Thus, there is an urgent need to find alternative pharmacological strategies to prevent or delay cataract formation.

The ephrin (Eph) receptors are the largest family of tyrosine kinases, comprising 14 Eph receptors that bind nine ephrin ligands [1]. Depending on the ligand, the Eph receptors are categorized as EphA or EphB. EphA2 (*EPHA2*) seems to play a bidirectional role in the progression of several cancers [2-5]. The extracellular domain of EPHA2 (N-terminal) consists of an ephrin-binding domain, a cysteine-rich domain, and two fibronectin III domains. The intracellular domain (C-terminal) comprises a tyrosine kinase domain, a sterile-α-motif (SAM) domain, and a PSD95/Dlg/ZO1 (PDZ) binding site (Figure 1). Since the first report of an association between *EPHA2* variants and cataract [6], *EPHA2* polymorphisms have been linked to congenital cataract [7–9] and age-related cataract (ARC) [10–12] in various populations. However, the mechanisms by which *EPHA2* polymorphisms result in cataract pathogenesis are unclear. For functional studies, we chose four evolutionarily conserved single nucleotide polymorphisms (SNPs) located in the intracellular domain of EPHA2 (i.e., rs35903225 [13], rs145592908, rs137853199 [6], and rs116506614 [14]). We refer to rs35903225 as M1,

Correspondence to: Jin Yang, Department of Ophthalmology, Eye & ENT Hospital of Fudan University, 83 Fenyang Road, Shanghai, China, 200031; Phone: 86-21-64377134; FAX: 86-21-64377151; email: jin_er76@hotmail.com

rs145592908 as M2, rs137853199 as M3, and rs116506614 as M4. M2 and M4 are located in the protein kinase domain, M1 is located right behind the protein kinase domain, and M3 is located in the SAM domain (Figure 1A). We found that M3 (c.2842G>T, p.G948W) could significantly decrease EPHA2 expression, while the mRNA levels were relatively stable among the four variants. These results are consistent with those of a previous study, which indicated that mutations in the SAM domain dramatically destabilize EPHA2 [15]. We confirmed that this destabilization is mediated by the ubiquitin–proteasomal pathway through a lysine-48 (K48)-specific ubiquitin linkage. Furthermore, we compared samples from patients with three types of ARC with normal controls and found that cortical cataract is associated with M3. Based on our results, we concluded that rs137853199 (M3) in the SAM domain could induce EPHA2 degradation, and this mutation is associated with cortical cataract in a small sample.

METHODS

Patient characteristics and sample collection: All procedures were reviewed and approved by the ethics committee of the Eye & ENT Hospital of Fudan University. The study adhered to the Association for Research in Vision and Ophthalmology (ARVO) statement on human subjects and the tenets of the Declaration of Helsinki. Informed consent was obtained from the patients in written form before collecting the blood samples. A total of 184 patients diagnosed with ARC between October 2015 and July 2016 AND who required surgery were enrolled in the study. Before surgery, routine ophthalmic examinations were conducted. Cataract type and severity were graded using the modified Lens Opacity Classification System III (LOCS III). Nuclear color status was graded by the same ophthalmologist based on slit-lamp images. All the patients were in the age range of 50–80 years and exhibited no other accompanying systemic, corneal, or retinal disease. The axial lengths of the patients with ARC who were included in this study were within the normal range (22–25 mm). Based on the results of ophthalmic examination, the patients were divided into three groups, which comprised 73 cortical cataract (CC) patients, 56 nuclear cataract (NC) patients, and 55 posterior subcapsular cataract (PSC) patients. We included 49 normal control subjects from the medical examination center of Jinshan Hospital, which is affiliated with Fudan University.

LEC transfection and knockdown: The lens epithelial cell (LEC) line SRA01/04 [16] was used for the cellular assays. This cell line was verified using short tandem repeat (STR)

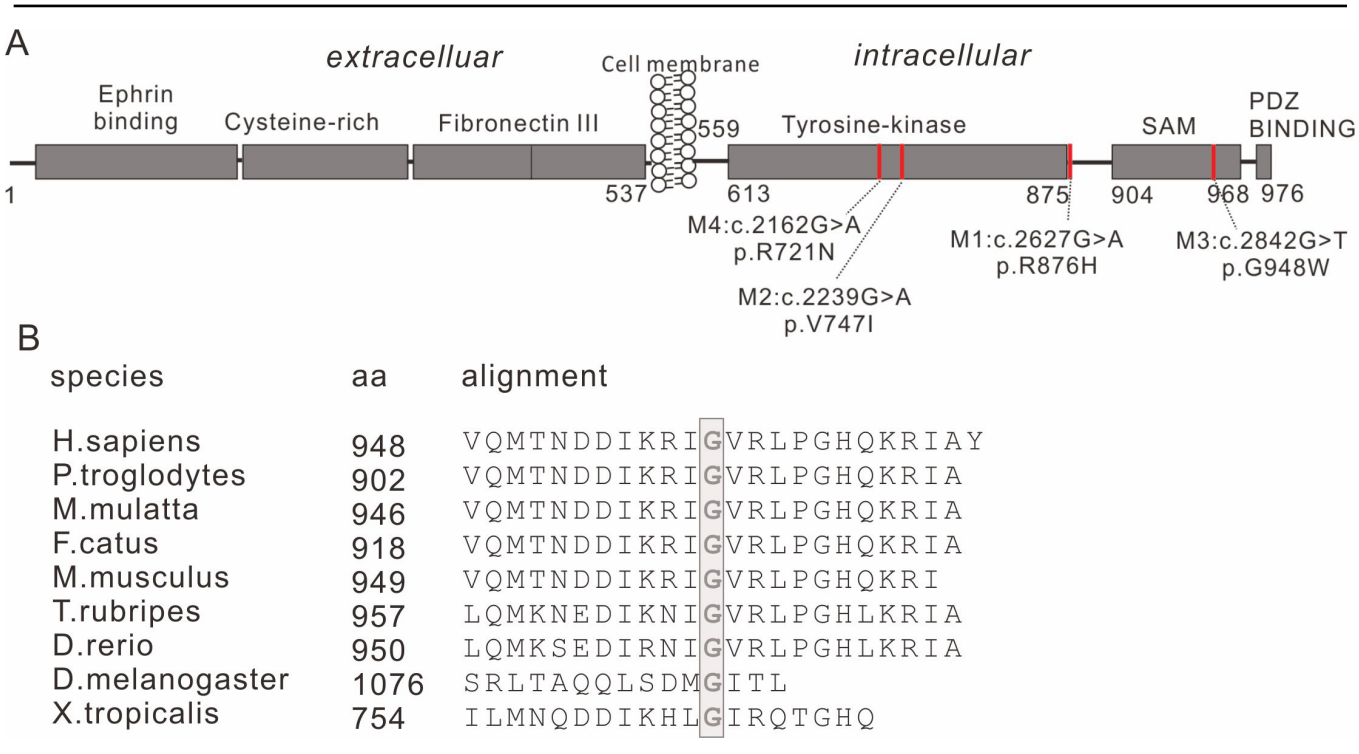

Figure 1. Schematic depicting the four mutated sites in EPHA2. **A**: The four mutated sites (M1–M4) are all located in the intracellular part of the protein. **B**: The M3 site (boxed column) is conserved across evolution. rs35903225, M1; rs145592908, M2; rs137853199, M3; rs116506614, M4.

analysis before usage; the identification report is provided in Appendix 1. SRA01/04 cells were cultured in Dulbecco's modified Eagle's medium (DMEM) medium (#11995, Gibco, Thermo Fisher Scientific, Waltham, MA) supplemented with 10% fetal bovine serum (FBS; #10099141, Gibco) under humidified air containing 5% CO_2 at 37 °C. All plasmids were purchased from Genechem (Shanghai, China). Wild-type (WT) and mutated *EPHA2* were cloned into the lentiviral vector GV365 (Ubi-MCS-3FLAG-CMV-EGFP; FLAG refers to the protein tag FLAG-tag (DYKDDDDK); EGFP refers to enhanced green fluorescent protein). The GV365 constructs were cotransfected with two helper plasmids, pHelper1.0 and pHelper2.0, into 293T cells. LECs were infected with lentivirus (10^8 TU/ml) in combination with polybrene (final concentration, 5 μg/ml) for 12 h, followed by replacement of the medium. The infected LECs were then cultured and collected for subsequent analysis.

To knock down the endogenous *EPHA2*, shRNAs targeting six unique sequences were constructed (sh1–sh6) using the lentiviral vector PHY-304 (hU6-MCS-CMV-Puro). Puromycin (2 μg/ml) was used to select the infected cells. Knockdown efficiency of the six shRNA candidates was analyzed using quantitative PCR (qPCR). The knockdown efficiency of sh4—which targeted the GGC TGA GCG TAT CTT CAT TGA sequence—was found to be the best among all six shRNAs.

Immunofluorescence: The LECs were fixed in 4% paraformaldehyde for 30 min and permeabilized with PBS (1X; 120 mM NaCl, 20 mM KCl, 10 mM $NaPO_4$, 5mM KPO_4 , pH 7.4) containing 0.03% Triton X-100 for 15 min, followed by blocking in PBS containing 5% goat serum and 0.1% bovine serum albumin (BSA) for 1 h. Cells were then probed overnight with the anti-FLAG antibody (#F1804, Sigma-Aldrich, Merck KGaA, Darmstadt, Germany; 1:100) at 4 °C, followed by incubation with Alexa Fluor 488-conjugated goat anti-mouse immunoglobulin G (IgG) and Hoechst 33,258 (1:2,000, Invitrogen, Thermo Fisher Scientific) and observed under a Zeiss microscope (Zeiss, Oberkochen, Germany).

MG132 and CQ treatment: Cells were seeded in six-well plates at a density that resulted in 50% confluency on the next day. MG132 (100 mM in dimethyl sulfoxide [DMSO]) was purchased from Merck (M7449, Darmstadt, Germany). Chloroquine (CQ; stock concentration, 100 mM; C6628, Merck) was reconstituted in filtered water (0.2 μm). When treated with MG132 (final concentration = 5 μM), cells underwent apoptosis and cell death after 24 h, whereas the CQ treatment (final concentration = 25 μM) induced no obvious changes. This observation is shown in Appendix 2. Based on this result, the LECs were treated with MG132 (5 μM) or CQ (25 μM) for 12 h.

Western blot: For western blots, cells collected at specific time points were lysed in radioimmunoprecipitation assay (RIPA) lysis buffer (R0278, Sigma) in the presence of a protease inhibitor cocktail (#78425, Thermo Scientific). The lysate was centrifuged at 12,000 ×*g* for 15 min at 4 °C, the supernatant was stored for the further analyses described below. The protein concentration was measured using a bicinchoninic acid (BCA) assay to enable equal protein loading on the gel. The protein samples were denatured in 5X loading buffer by boiling at 100 °C for 5 min in a dry bath. The samples were separated on a 10% sodium dodecyl sulfate polyacrylamide gel electrophoresis (SDS-PAGE) gel and transferred onto a 0.45 μm pore size polyvinylidene difluoride (PVDF) membrane (IPVH00010, Merck). The membrane was blocked using 5% nonfat milk prepared in Tris-Buffered Saline with 0.1% Tween (TBS-T) for 1 h at room temperature. Next, the PVDF membranes were probed overnight with the following primary antibodies at 4 °C: EPHA2 (#6997; CST, Ipswich, MA), β-catenin (ab32572; Abcam, UK), β-actin (A3854; Sigma), Ub (P4D1; sc-8017; Santa Cruz Biotechnology, Dallas, Texas), Ub-K63 (ab179434, Abcam, Cambridge, MA), and Ub-K48 (ab140601, Abcam). On the next day, the membranes were washed three times (10 min each) with TBS-T and probed for 1 h with peroxidase-conjugated goat anti-mouse IgG (H^+L) or anti-rabbit IgG (H^+L; Yeasen, China). Signals were developed using Super Signal West Pico (NCI5079, Thermo Scientific), and the images were detected using a Kodak Imaging System. Protein signals were quantitated using ImageJ.

qPCR: Total RNA was extracted using TRIzol (15,596, Thermo Fisher) and measured on a NanoDrop 2000 (Thermo Fisher). Reverse transcription was performed using an reverse transcription kit (KR106–02, Tiangen, China), and qPCR was performed using SYBR Premix (FP205–02, Tiangen). qPCR was performed on an ABI 7500 PCR machine, and data were analyzed using the ABI 7500 software v2.0.6 (Life Technologies). The following primer sequences were used: *EPHA2*, 5'- GAG AAG GAT GGC GAG TTC AG -3' (forward) and 5'- AGG TTG CTG TTG ACG AGG AT -3' (reverse); *β-actin*, 5'- TTG TTA CAG GAA GTC CCT TGC C -3' (forward) and 5'- ATG CTA TCA CCT CCC CTG TGT G -3' (reverse).

Coimmunoprecipitation: Immunoprecipitation (IP) was performed using anti-EPHA2 (#6997; CST) or anti-FLAG (#F1804; Sigma) antibody. Total protein (100 μg) was precleared using Protein A agarose (sc-2003, Santa Cruz Biotechnology) for 2 h at room temperature with slow rotation. Next, 1 μg of anti-EPHA2 or anti-FLAG antibody was

used to probe the precleared protein by mixing overnight at 4 °C; this step was followed by centrifugation at 1,000 ×g for 1 min, and the supernatant was discarded. The pulled beads were washed three times with cold lysis buffer, and the proteins were eluted by boiling in 2X SDS loading buffer. Western blots for checking the expression of EPHA2, Ub, Ub(K48), and Ub(K63) were performed, as described above.

IP-MS and bioinformatics analysis: IP-MS was performed using an MS-compatible magnetic IP kit (#90409, Thermo Scientific) per the manufacturer's instructions. Briefly, cell lysate (500 µg total protein; WT-EPHA2 or M3-EPHA2 overexpressing cells) was incubated with 5 µg of anti-FLAG antibody at 4 °C with mixing overnight. Next, 0.25 mg Protein A/G magnetic beads were added to the sample/antibody mixture and incubated at room temperature for 1 h with mixing. Unbound samples were discarded after the beads were collected with a magnetic stand. The protein–bead mixture was washed and eluted using the IP-MS elution buffer. The samples were then processed for MS by reduction, alkylation, and trypsin digestion. The peptides were analyzed by liquid chromatography-tandem MS on a Q Exactive mass spectrometer (Thermo Scientific).

MS data were analyzed using MaxQuant 1.6.2.3 software and searched against the human Swiss-Prot database [17]. Carbamidomethyl cysteine was searched as a fixed modification, and oxidized methionine and protein N-term acetylation were set as variable modifications. The minimum peptide length was set at seven residues. The tolerances of the first and main searches for peptides were set at 20 and 4.5 ppm, respectively. Protein intensity was determined using the intensity-based absolute quantification (iBAQ) method in MaxQuant. Two independent experiments were performed. A total of 87 proteins were identified in the WT group in both experiments. The molecular function and pathway enrichment were analyzed using Panther.

Transwell migration assay: Cells (5,000/chamber) were seeded in the upper chamber of transwell inserts (#3422; pore size, 8 µm; Corning, Kennebunk, ME) in 100 µl serum-free medium. Culture medium (600 µl) supplemented with 10% fetal bovine serum was added to the lower chamber as a chemoattractant. After 24 h, the upper surface of the insert was gently scratched with a cotton swab. Cells invading the lower chamber were fixed with 4% paraformaldehyde and stained with crystal violet. The number of invading cells was counted under a microscope. Five random fields were analyzed for each insert.

Structural modeling: The structural changes induced by M3 were predicted and optimized using Schrödinger software [18]. The structure was drawn using PyMOL Molecular Graphics System software (Version 1.3 Schrödinger, LLC).

Sanger sequencing: Peripheral blood (1–2 ml) was collected from the enrolled patients. DNA was prepared from the blood samples deposited in the issue library of Eye & ENT Hospital of Fudan University (also called EENT Biobank; Shanghai, China), and its concentration was measured using a NanoDrop 2000 (Thermo Fisher Scientific); 100 ng DNA was used for molecular analysis. A 518 bp DNA fragment was amplified using PCR (5'- GTT GAG GCT TCT GTC GTT T -3' (forward) and 5'- GCC AGG GTG TCA TCC GAG -3' (reverse)). The amplified fragment was sequenced in both directions using the primers described above.

Statistical analysis: A two-tailed Student *t* test was used to compare quantitative data between the two groups, and a chi-square test was used to compare the sample distribution between the groups (GraphPad Prism version 7.00 for Windows, GraphPad Software, La Jolla, CA). Data are presented as the mean ± standard deviation (SD), and p-values < 0.05 were considered statistically significant.

RESULTS

Expression pattern of the EPHA2 mutants: We cloned the four *EPHA2* point mutants (M1–M4; Figure 1A) and the WT (all tagged with FLAG and EGFP) into lentiviral vectors. LECs were transduced, and the transfection efficiency was confirmed based on EGFP fluorescence (Appendix 3 and Appendix 4).

We analyzed the expression of the EPHA2 mutants using western blotting (Figure 2A). Semiquantitative analysis was used to analyze the fold change in density compared with the WT (Figure 2B). As shown in Figure 2B, we observed a significant decrease in M3-EPHA2 expression compared with WT-EPHA2, using the anti-FLAG antibody, which is specific to the ectopically expressed EPHA2. Interestingly, as shown in Figure 1B, the M3 site was conserved across evolution. Unlike the protein levels, the mRNA levels of the mutants were relatively stable among the four variants and comparable to those of the WT (Appendix 5). These results indicated that M3 decreased EPHA2 expression primarily at the post-transcriptional level.

The cellular localization of ectopically expressed FLAG-tagged M3-EPHA2 and WT-EPHA2 was investigated using immunofluorescence. As shown in Figure 2C, ectopically expressed WT-EPHA2 is mainly localized to the plasma membrane. However, the signal for M3-EPHA2 was weak, and therefore, it was difficult to determine its exact localization within the cell.

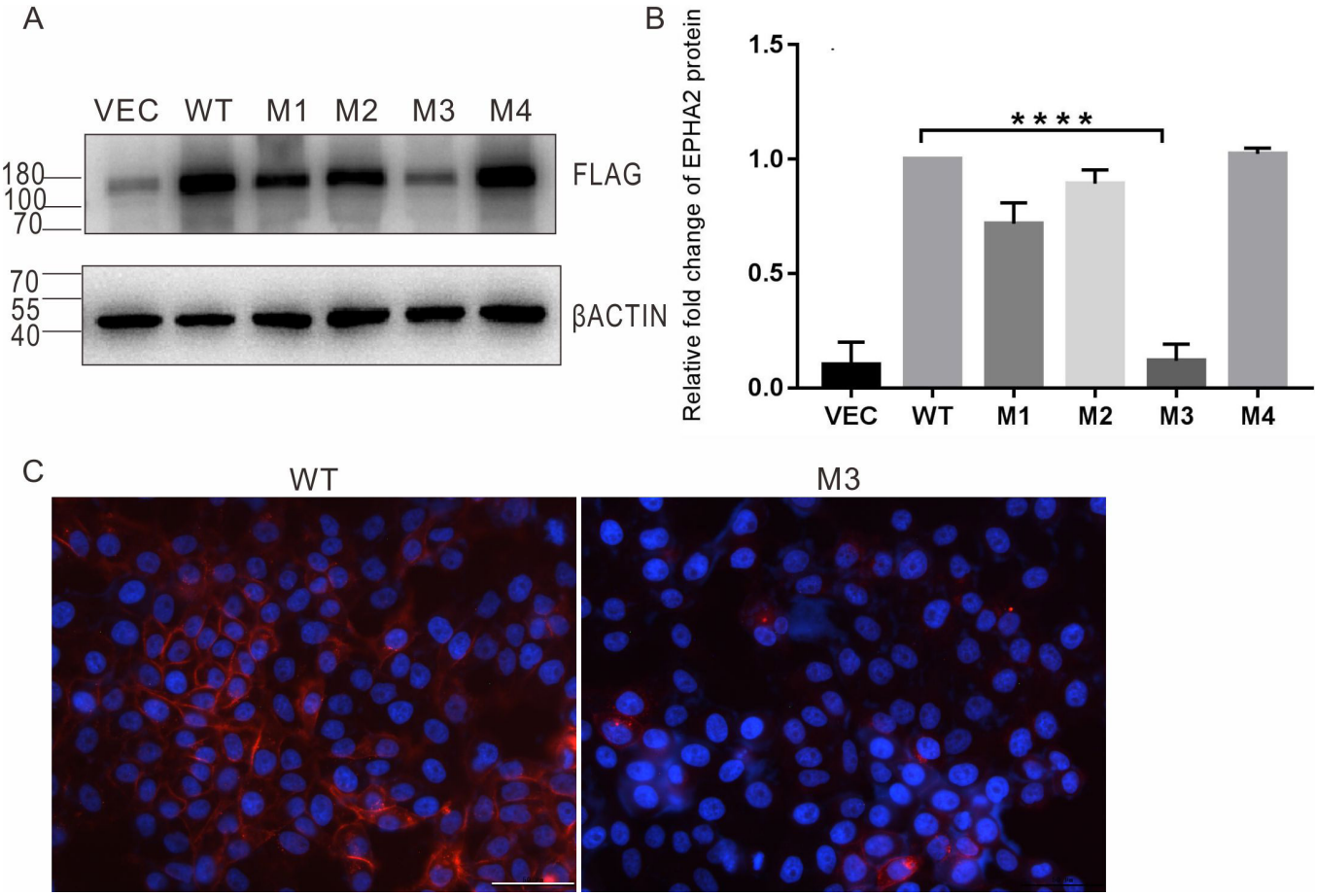

Figure 2. M3 reduces EPHA2 levels. **A**: Western blot using anti-FLAG antibody. VEC: vector only. **B**: Semiquantitative analysis based on the western blot. The relative band intensity was calculated in two steps. First, the values corresponding to the intensity of the FLAG band were divided by those corresponding to the intensity of the β-actin band, and second, these values were divided by the values obtained for the WT. For the WT, this value was set to 1. The data are the average from three independent experiments; the western blot images are provided in Appendix 9. Endogenous control: β-actin, sample control: WT, n = 3, ****p<0.0001. **C**: Immunofluorescence of WT-EPHA2 and M3-EPHA2, red: FLAG, blue: nuclear, scale bar: 50 µm.

MG132 and CQ recovered M3-EPHA2 degradation: Based on the decreased expression of M3-EPHA2, we focused on this mutant for further study. LECs overexpressing M3-EPHA2 or WT-EPHA2 were independently treated for 12 h with MG132 (a proteasome inhibitor) or CQ (a lysosomal degradation inhibitor). Western blotting revealed that, whereas MG132 increased the expression of both M3-EPHA2 and WT-EPHA2, the fold-change increase in the expression of M3-EPHA2 was significantly higher than that of WT-EPHA2 (Figure 3). Meanwhile, CQ did not significantly increase the expression of either M3-EPHA2 or WT-EPHA2. These data indicate that the significantly low expression of M3-EPHA2—compared with that of WT-EPHA2—may be attributed to a higher degree of proteasomal degradation.

Higher levels of K48-linked ubiquitination were observed in M3-EPHA2: To better understand the degradation of WT-EPHA2 and M3-EPHA2, we performed immunoprecipitation experiments in cells ectopically expressing WT-EPHA2 or M3 EPHA2. We coimmunoprecipitated the ectopically expressed EPHA2 using the anti-FLAG and anti-EPHA2 antibodies. Western blotting revealed that K48-linked—but not K63-linked—ubiquitin moieties were enriched in M3-EPHA2 (compared with WT-EPHA2; Figure 4). These results confirmed that both M3-EPHA2 and WT-EPHA2 undergo ubiquitin-mediated proteasomal degradation. Moreover, the M3 enhanced the degradation of EPHA2 by increasing the levels of K48-linked ubiquitination.

M3 reduced cell migration: The transwell assays revealed that EPHA2 knockdown reduced the migration of LECs (Figure 5A-B). Remarkably, while the overexpression of WT-EPHA2 could rescue the EPHA2-knockdown–induced reduction in cell migration, M3-EPHA2 could not do so (Figure 5C-D).

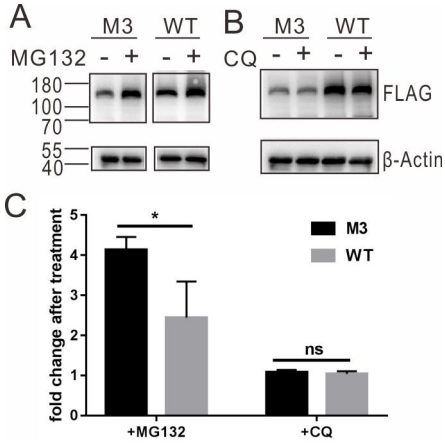

Figure 3. MG132 recovered M3-EPHA2 to a greater level than WT did. After treatment with MG132 or CQ, the levels of M3 and WT EPHA2 were analyzed by western blotting. The data depict the semiquantitative analysis based on the western blots, which are the averages from three independent experiments. The relative band intensity was calculated in two steps. First, the values corresponding to the intensity of the FLAG band were divided by those corresponding to the intensity of the β-actin band, and second, the value in the treatment group (+) was divided by the value in the untreated group (–). The western blot images from the three experiments are provided in Appendix 10. Endogenous control: β-actin, sample control: untreated group, n = 3, *p<0.05. ns: not significant.

The quantified results of the five random microscopic fields are presented in Figure 5E. Next, we examined the expression of β-catenin, a key regulator of cell migration, using western blotting. We found that the expression of β-catenin significantly decreased in LECs overexpressing M3-EPHA2 compared with that in LECs overexpressing WT-EPHA2 (Figure 5F-G).

M3 induced structural changes in EPHA2 and recruited unique proteins: As shown in Figure 6, M3 induced a clear change in the protein structure around p.948, resulting in an outward protuberance (Figure 6B,D). A previous study has shown that mutations in the SAM domain reduce protein solubility [15]. Therefore, we speculated that this change may be the driving factor that reduces the solubility of EPHA2, contributing to a higher degree of protein degradation (Figure 2).

To examine the proteins that directly interact with M3-EPHA2 and WT-EPHA2, we performed IP-MS. All the identified proteins are listed in Appendix 6. The results showed that 87 proteins specifically bind to WT-EPHA2 but not to M3-EPHA2. Meanwhile, 78 proteins specifically bind to M3-EPHA2 (Appendix 6). The main molecular functions associated with the proteins in either group included binding and catalysis, while their main protein class was protein-modifying enzyme. Figure 7 shows the main classes of the proteins that specifically bind to WT-EPHA2.

Patients with cortical cataract exhibit higher M3 frequency: We isolated genomic DNA from the blood samples of 49 control subjects and 184 ARC patients (including 73 cortical cataract patients, 56 nuclear cataract patients, and 55 PSC patients). Sanger sequencing of the *EPHA2* SAM region that covers the M3 site revealed that the minor allele frequency at M3 was significantly higher in patients with cortical cataract than in controls (Table 1). However, when the minor allele frequency—at M3—in the full sample of ARC patients was compared with that in the controls, no significant difference was found (Appendix 7). Together, these data suggest that M3 can potentially affect the progression of cortical cataracts.

DISCUSSION

M3 induced structural changes in EPHA2 and resulted in its degradation: Transgenic mice that are homozygous for *EPHA2* deletion develop cortical cataract around the age of 3–6 months [14]—equivalent to a human age of 20–30 years—suggesting that, in cortical cataracts, the role of

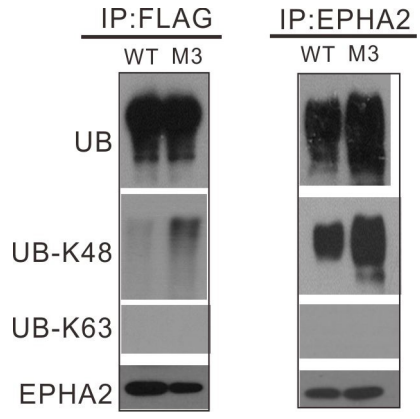

Figure 4. Identification of the ubiquitin lysine involved in the EPHA2 proteolysis. Proteins isolated from cells overexpressing WT or M3-EPHA2 were immunoprecipitated with FLAG or EPHA2 antibody, and western blot was performed using three ubiquitin linkage-specific antibodies.

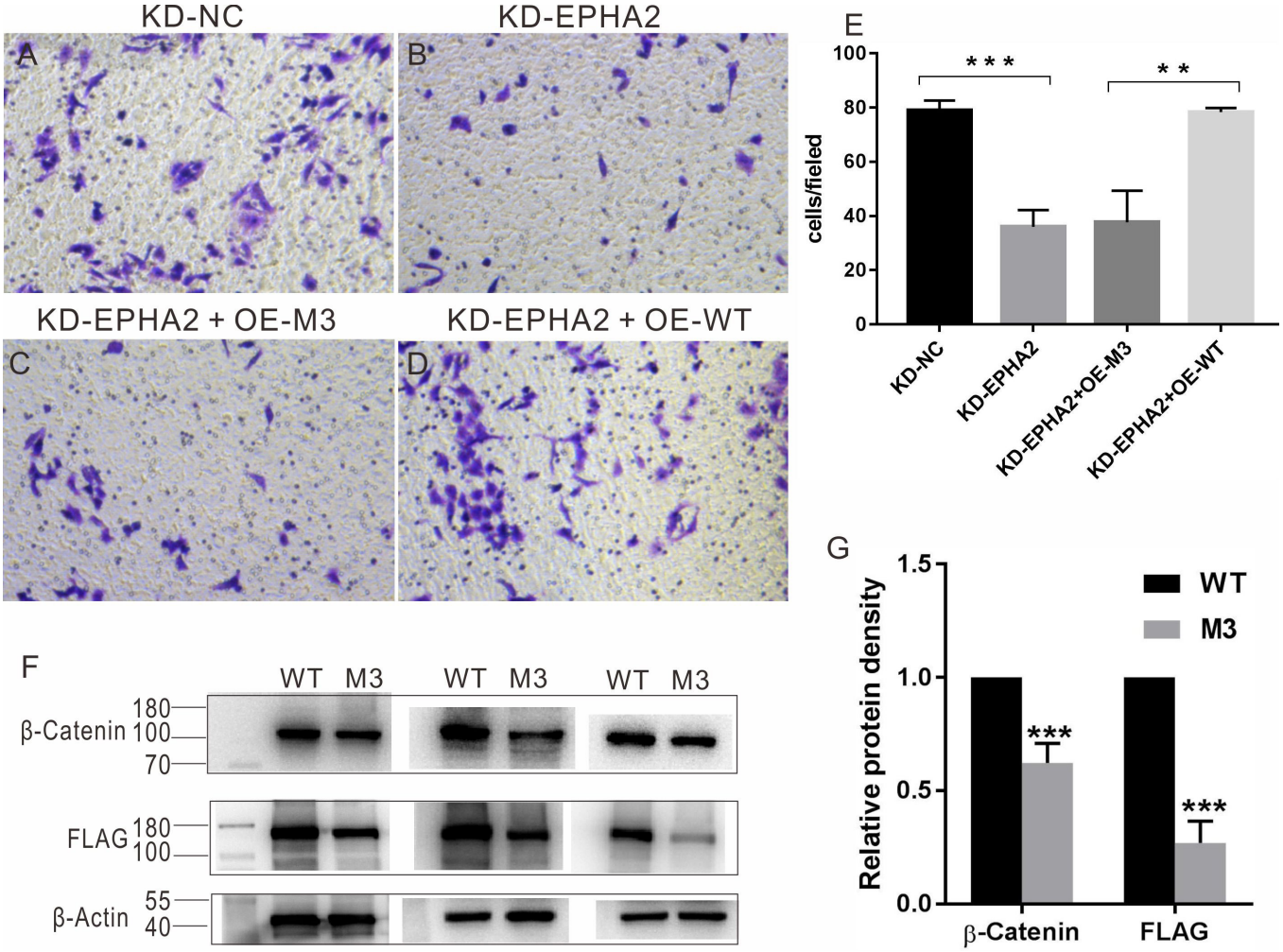

Figure 5. EPHA2 is essential for maintaining cell migration ability. **A**, **B**: Transwell assays, EPHA2 knockdown reduced cell migration. KD-NC: knockdown using the negative control siRNA, KD-EPHA2: knockdown of EPHA2, KD-EPHA2+OE-M3: knockdown of EPHA2 + overexpression of M3-EPHA2, KD-EPHA2+OE-WT: knockdown of EPHA2 + overexpression of WT-EPHA2. **C**, WT-EPHA2 overexpression restored cell migration ability to a normal level (**A**). **D**: M3-EPHA2 overexpression did not rescue the reduced cell migration ability of the EPHA2 kDa cells . **E**: Quantification of the transwell assay images; five fields were counted in each insert well, n = 5, ***p<0.001, **p<0.01. **F**: Western blot images showing that the level of β-catenin significantly decreased in LECs overexpressing M3-EPHA2. **G**: Quantification of the protein levels based on western blots in **F**. The relative band intensity was calculated in two steps. First, the values corresponding to the intensity of the β-catenin band or the FLAG band were divided by those corresponding to the intensity of the β-actin band, and second, these values were divided by the values obtained for the WT sample. For the WT, this value was set as 1. Endogenous control: β-actin, sample control: WT-EPHA2 overexpressing group, n = 3, ***p<0.001.

EPHA2 in the maintenance of lens transparency comes in at a later stage (compared with congenital cataracts). In humans, approximately 20 *EPHA2* point mutations have been reported to be responsible for the development of congenital cataracts, suggesting that *EPHA2* functions during the early stages of transparent lens development. However, studies using genetically modified animal models, particularly mouse models, are necessary to provide confirmative evidence of how these mutations lead to the development of disease.

M3 is located in the SAM domain of EPHA2, which is highly conserved in all Eph receptors. The M3-induced surface protrusion (Figure 6) could play an important role in aiding the degradation of this EPHA2 mutant. Treatment with the proteasomal inhibitor, MG132, resulted in increased expression of M3-EPHA2 (4.1-fold) and WT-EPHA2 (2.4-fold; Figure 3). This result suggests that the proteasomal pathway is involved in the degradation of M3-EPHA2.

Ubiquitination is a well-studied posttranslational modification. Usually, ubiquitin chains are formed via bonds

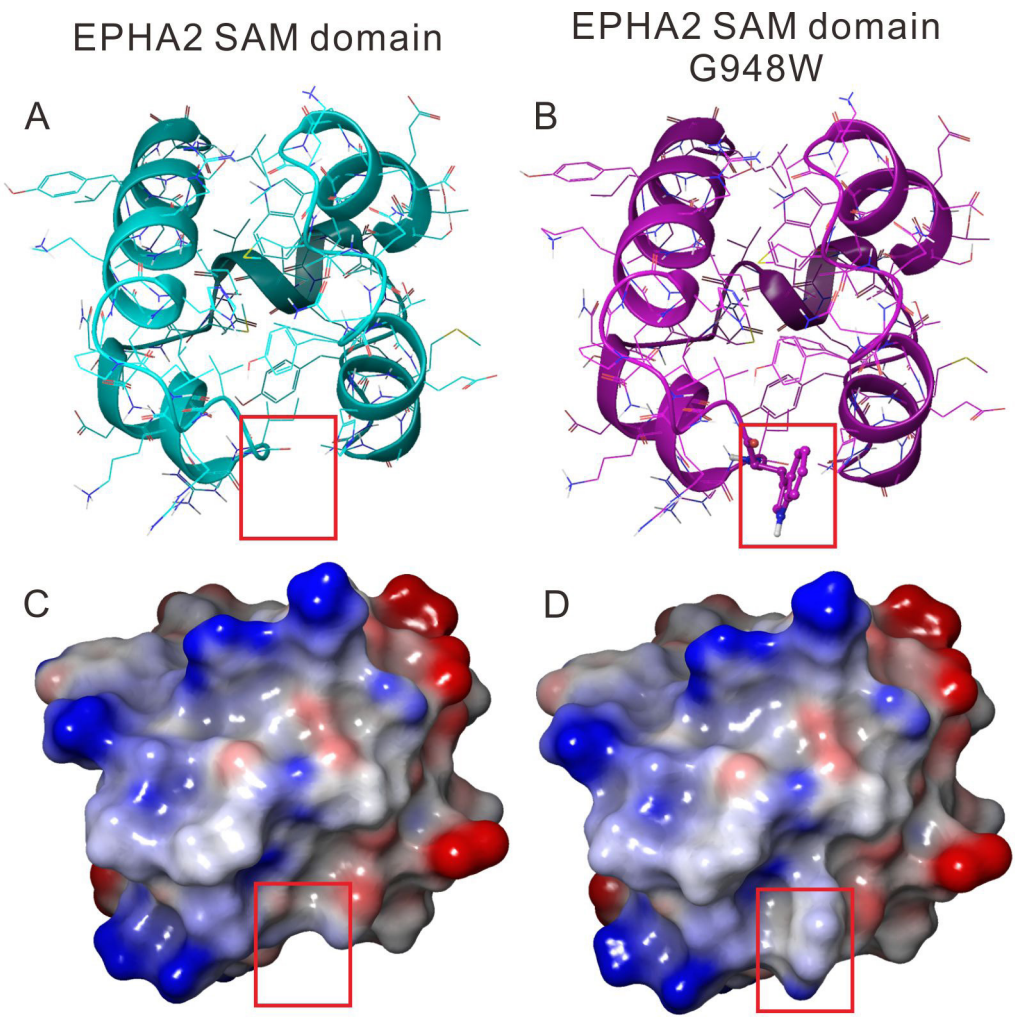

Figure 6. The predicted structure of WT-EPHA2 and M3-EPHA2. **A**, **B**. Loop-helix structures. **C**, **D**: Surface structures. The red box highlights the structural differences between WT-EPHA2 and M3-EPHA2.

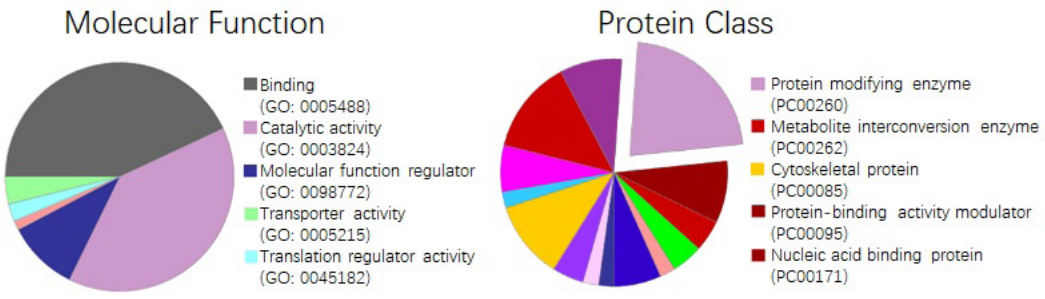

Figure 7. WT-EPHA2 and M3-EPHA2 bind different proteins. The binding proteins were identified by IP-MS. The 87 proteins that specifically bind to WT-EPHA2 are enriched under the molecular function “binding” and “catalytic activity” and under the protein class “protein-modifying enzyme.”

Table 1. Higher mutation rate of M3 rs137853199 in cortical cataract patients.

SNPs	Allele	CC group n (%)	Control group n (%)	P value	OR for minor allele (95% CI)
rs137853199	C	133(77.4%)	92(93.9%)	0.00058	1.223 (0.897–1.561)
	T	41(22.6%)	21(6.1%)		
	Genotype			0.0048	-
	C C	45(61.6%)	43(87.8%)		
	C T	23(31.5%)	6(12.2%)		
	T T	5(6.8%)	0(0.0%)		

between a lysine residue (K) in one ubiquitin molecule and a C-terminal diglycine in another. K48 and K63 are the two major ubiquitin linkage types. While K48-linked ubiquitin chains lead to the proteasomal degradation of conjugated proteins, K63-linked chains are involved in the recruitment of DNA repair enzymes, cell signaling, and endocytosis [19]. Here, we found that M3-EPHA2 is proteasomally degraded via polyubiquitinylation through the K48 linkage (Figure 4), which explains the significantly low expression of M3-EPHA2.

EPHA2 overexpression is reported to promote cell migration in a ligand-independent manner [2,15], and endothelial cells from EphA2-deficient mice are known to display an impaired metastatic progression of tumors [20]. In this study, we found that knockdown of EPHA2 significantly reduced cell migration. When WT-*EPHA2* and M3-*EPHA2* were overexpressed in the EPHA2-knockdown cells, only WT-EPHA2 could rescue the defect in cell migration. Moreover, the dramatic decrease in β-catenin levels in LECs overexpressing M3-EPHA2 indicated that this mutant affects cell migration through the canonical Wnt pathway. Using IP-MS, we found that WT-EPHA2 and M3-EPHA2 interacted with different proteins. While 87 proteins specifically bound to WT-EPHA2 (Figure 7), 78 proteins specifically bound to M3-EPHA2 (Appendix 6). The function of most proteins depends on how they bind to other proteins. The M3 mutation of *EPHA2* (c.2842G>T, p.G948W) causes protein structural change and altered binding ability to ligands. The different binding proteins are highly enriched in “modifying enzymes” in terms of protein class and “binding” and “catalysis” in terms of molecular function. For example, in the group of proteins with the function of “ubiquitin binding,” WT-EPHA2 binds (ubiquitin protein ligase E3C (UBE3C), whereas M3-EPHA2 binds tripartite motif 23 (TRIM23). Both UBE3C and TRIM23 act as ubiquitin ligase. UBE3C accepts ubiquitin from the E2 ubiquitin-conjugating enzyme UBE2D1 and transfers the ubiquitin to targeted substrates; TRIM23 mediates atypical lysine 27 (K27)-linked polyubiquitin conjugation to nuclear factor κB (NFκB) essential modulator (NEMO), which plays an important role in the NFκB pathway. Such different binding abilities should contribute to the increased degradation of M3-EPHA2.

Association of EPHA2 rs137853199 with cataract: All four SNPs explored in this study are evolutionarily conserved and located close to the C-terminal (Figure 1). We found that, among these four SNPs, rs137853199 (c.2842G>T, p.G948W)—which was first identified in a Caucasian family with posterior polar cataract [6]—could result in significant EPHA2 degradation. In addition, in our case-controlled study, this SNP was found to be associated with age-related cortical cataract (p = 0.00058, Table 1).

The 2004 Beaver Dam Eye Study established a linkage between cortical cataract and markers on chromosome 1p36, including *EPHA2* [21]. Since then, several *EPHA2* mutations associated with different types of cataracts have been identified. In congenital cataracts, *EPHA2* mutations are most frequently localized within the SAM domain [6,8,9,22,23], followed by the fibronectin type III domain [24-28] and the tyrosine kinase domain [27,29,30]. Seven SNPs have been reported to be associated with ARC (Appendix 8). Six of these are associated with cortical cataract, suggesting that *EPHA2* is more likely to be involved in the pathogenesis of this specific type of cataract. One explanation for why the mutation identified in congenital cataracts is associated with ARC is that the penetrance of this mutation is relatively low. Alternatively, the compound heterozygosity of *EPHA2* is also likely to contribute to disease pathogenesis. In summary, this study provides new insights into the mechanism by which *EPHA2* point mutations affect protein degradation and provides evidence of the association between *EPHA2* rs137853199 and cortical cataracts.

APPENDIX 1. STR ANALYSIS.

To access the data, click or select the words “Appendix 1.”

APPENDIX 2. MG132 TREATMENT INDUCED CELLS DEATH.

To access the data, click or select the words "Appendix 2." After MG132 treatment (final conc.=5 μM), cells were observed under a fluorescence microscope. Here the images of WT-EPHA2 overexpressing cells were presented (all the other types of EPHA2 overexpressing cells showed similar changes of cell death). The upper lanes, bright light images; lower lanes, fluorescent images. Scale bar, 200 μm.

APPENDIX 3. FLUORESCENT MICROSCOPY INDICATED THE TRANSFECTION EFFICIENCY

To access the data, click or select the words "Appendix 3." The green fluorescent images of the cells overexpressing WT, M1-M4-EPHA2 and vector plasmid only (as the constructs contain EGFP). Scale bar, 200 μm.

APPENDIX 4. FLUORESCENT MICROSCOPY ANALYSIS CONFIRMS THE TRANSFECTION EFFICIENCY.

To access the data, click or select the words "Appendix 4." Upper lane: bright-field, green fluorescent field and merged images of cells overexpressing WT-EPHA2; lower lane: bright-field, green fluorescent field and merged images of cells overexpressing M3-EPHA2. Scale bar: 500 μm.

APPENDIX 5. THE MRNA LEVELS OF *EPHA2* M1-M4 VARIANTS WERE COMPARABLE.

To access the data, click or select the words "Appendix 5." The mRNA levels were measured using qPCR. Endogenous gene control: *β-actin*, sample control: WT, n=3. rs35903225, M1; rs145592908, M2; rs137853199, M3; rs116506614, M4. ns: not significant.

APPENDIX 6. THE LIST OF PROTEINS THAT SPECIFICALLY BIND TO WT OR M3-EPHA2.

To access the data, click or select the words "Appendix 6."

APPENDIX 7. NO SIGNIFICANT DIFFERENCE WAS FOUND AT RS137853199 WHEN TOTAL ARC PATIENTS WERE ANALYZED.

To access the data, click or select the words "Appendix 7."

APPENDIX 8. THE SEVEN SNPS ASSOCIATED WITH AGE-RELATED CATARACT.

To access the data, click or select the words "Appendix 8."

APPENDIX 9. THE THREE EXPERIMENTAL REPEATS OF WESTERN BLOTS TO MEASURE THE LEVELS OF ECTOPICALLY EXPRESSED EPHA2.

To access the data, click or select the words "Appendix 9." Western blot experiments to present the protein level of WT and M1-M4-EPHA2. The "VEC" lane is the blotting result using proteins from cells overexpressing vector plasmid. Endogenous control: β-Actin.

APPENDIX 10. THE THREE EXPERIMENTAL REPEATS OF WESTERN BLOTS TO MEASURE TO THE PROTEIN CHANGES IN M3-EPHA2 AND WT-EPHA2 AFTER MG132 OR CQ TREATMENT.

To access the data, click or select the words "Appendix 10." After treatment of MG132 or CQ, the levels of M3 and WT EPHA2 were analyzed by western blotting. (+): the treatment group, (-): the untreated group. Endogenous control: β-Actin

ACKNOWLEDGMENTS

This work was supported by the Shanghai Natural Science Foundation, grant number 16ZR1405200. Dr. Jin Yang (jin_er76@hotmail.com) and Dr. Yi Lu (luyieent@126.com) are co-corresponding authors of this work.

REFERENCES

1. Walker-Daniels J, Hess AR, Hendrix MJ, Kinch MS. Differential regulation of EphA2 in normal and malignant cells. Am J Pathol 2003; 162:1037-42. [PMID: 12651595].
2. Miao H, Li DQ, Mukherjee A, Guo H, Petty A, Cutter J, Basilion JP, Sedor J, Wu J, Danielpour D, Sloan AE. EphA2 mediates ligand-dependent inhibition and ligand-independent promotion of cell migration and invasion via a reciprocal regulatory loop with Akt. Cancer Cell 2009; 16:9-20. [PMID: 19573808].
3. Kaenel P, Mosimann M, Andres AC. The multifaceted roles of Eph/ephrin signaling in breast cancer. Cell Adhes Migr 2012; 6:138-47. [PMID: 22568950].
4. Vaught D, Brantley-Sieders DM, Chen J. Eph receptors in breast cancer: roles in tumor promotion and tumor suppression. Breast Cancer Res 2008; 10:217-[PMID: 19144211].
5. Pasquale EB. Eph receptors and ephrins in cancer: bidirectional signalling and beyond. Nat Rev Cancer 2010; 10:165-80. [PMID: 20179713].
6. Shiels A, Bennett TM, Knopf HLS, Maraini G, Li AR, Jiao XD, Hejtmancik JF. The EPHA2 gene is associated with cataracts linked to chromosome 1p. Mol Vis 2008; 14:2042-55. [PMID: 19005574].
7. Reis LM, Tyler RC, Semina EV. Identification of a novel C-terminal extension mutation in EPHA2 in a family affected

with congenital cataract. Mol Vis 2014; 20:836-42. [PMID: 24940039].

8. Zhang T, Hua R, Xiao W, Burdon KP, Bhattacharya SS, Craig JE, Shang D, Zhao X, Mackey DA, Moore AT, Luo Y. Mutations of the EPHA2 receptor tyrosine kinase gene cause autosomal dominant congenital cataract. Hum Mutat 2009; 30:E603-11. [PMID: 19306328].

9. Dave A, Laurie K, Staffieri SE, Taranath D, Mackey DA, Mitchell P, Wang JJ, Craig JE, Burdon KP, Sharma S. Mutations in the EPHA2 gene are a major contributor to inherited cataracts in South-Eastern Australia. PLoS One 2013; 8:e72518-[PMID: 24014202].

10. Tan W, Hou S, Jiang Z, Hu Z, Yang P, Ye J. Association of EPHA2 polymorphisms and age-related cortical cataract in a Han Chinese population. Mol Vis 2011; 17:1553-8. [PMID: 21686326].

11. Zhang H, Zhong J, Bian Z, Fang X, Peng Y, Hu Y. Association between polymorphisms of OGG1, EPHA2 and age-related cataract risk: a meta-analysis. BMC Ophthalmol 2016; 16:168-[PMID: 27681698].

12. Celojevic D, Abramsson A, Seibt Palmer M, Tasa G, Juronen E, Zetterberg H, Zetterberg M. EPHA2 polymorphisms in estonian patients with age-related cataract. Ophthalmic Genet 2016; 37:14-8. [PMID: 24673449].

13. Masoodi TA, Shammari SA, Al-Muammar MN, Almubrad TM, Alhamdan AA. Screening and structural evaluation of deleterious Non-Synonymous SNPs of ePHA2 gene involved in susceptibility to cataract formation. Bioinformation 2012; 8:562-7. [PMID: 22829731].

14. Jun G, Guo H, Klein BE, Klein R, Wang JJ, Mitchell P, Miao H, Lee KE, Joshi T, Buck M, Chugha P. EPHA2 is associated with age-related cortical cataract in mice and humans. PLoS Genet 2009; 5:e1000584-[PMID: 19649315].

15. Park JE, Son AI, Hua R, Wang L, Zhang X, Zhou R. Human cataract mutations in EPHA2 SAM domain alter receptor stability and function. PLoS One 2012; 7:e36564-[PMID: 22570727].

16. Ibaraki N, Chen SC, Lin LR, Okamoto H, Pipas JM, Reddy VN. Human lens epithelial cell line. Exp Eye Res 1998; 67:577-85. [PMID: 9878220].

17. Tyanova S, Temu T, Cox J. The MaxQuant computational platform for mass spectrometry-based shotgun proteomics. Nat Protoc 2016; 11:2301-19. [PMID: 27809316].

18. Schrödinger-Release. Schrödinger Release 2017–3. Prime, Schrödinger, LLC, New York, NY. 2017.

19. Walczak H, Iwai K, Dikic I. Generation and physiological roles of linear ubiquitin chains. BMC Biol 2012; 10:23-[PMID: 22420778].

20. Brantley-Sieders DM, Fang WB, Hicks DJ, Zhuang G, Shyr Y, Chen J. Impaired tumor microenvironment in EphA2-deficient mice inhibits tumor angiogenesis and metastatic progression. FASEB J 2005; 19:1884-6. [PMID: 16166198].

21. Iyengar SK, Klein BE, Klein R, Jun G, Schick JH, Millard C, Liptak R, Russo K, Lee KE, Elston RC. Identification of a major locus for age-related cortical cataract on chromosome 6p12-q12 in the Beaver Dam Eye Study. Proc Natl Acad Sci USA 2004; 101:14485-90. [PMID: 15452352].

22. Bu J, He S, Wang L, Li J, Liu J, Zhang X. A novel splice donor site mutation in EPHA2 caused congenital cataract in a Chinese family. Indian J Ophthalmol 2016; 64:364-8. [PMID: 27380975].

23. Li D, Wang S, Ye H, Tang Y, Qiu X, Fan Q, Rong X, Liu X, Chen Y, Yang J, Lu Y. Distribution of gene mutations in sporadic congenital cataract in a Han Chinese population. Mol Vis 2016; 22:589-98. [PMID: 27307692].

24. Javadiyan S, Lucas SEM, Wangmo D, Ngy M, Edussuriya K, Craig JE, Rudkin A, Casson R, Selva D, Sharma S, Lower KM. Identification of novel mutations causing pediatric cataract in Bhutan, Cambodia, and Sri Lanka. Mol Genet Genomic Med 2018; 6:555-64. [PMID: 29770612].

25. Sun W, Xiao X, Li S, Guo X, Zhang Q. Exome sequencing of 18 Chinese families with congenital cataracts: a new sight of the NHS gene. PLoS One 2014; 9:e100455-[PMID: 24968223].

26. Gillespie RL, O'Sullivan J, Ashworth J, Bhaskar S, Williams S, Biswas S, Kehdi E, Ramsden SC, Clayton-Smith J, Black GC, Lloyd IC. Personalized diagnosis and management of congenital cataract by next-generation sequencing. Ophthalmology 2014; 121:2124-37. [PMID: 25148791].

27. Patel N, Anand D, Monies D, Maddirevula S, Khan AO, Algoufi T, Alowain M, Faqeih E, Alshammari M, Qudair A, Alsharif H. Novel phenotypes and loci identified through clinical genomics approaches to pediatric cataract. Hum Genet 2017; 136:205-25. [PMID: 27878435].

28. Aldahmesh MA, Khan AO, Mohamed JY, Hijazi H, Al-Owain M, Alswaid A, Alkuraya FS. Genomic analysis of pediatric cataract in Saudi Arabia reveals novel candidate disease genes. Genet Med 2012; 14:955-62. [PMID: 22935719].

29. Kaul H, Riazuddin SA, Shahid M, Kousar S, Butt NH, Zafar AU, Khan SN, Husnain T, Akram J, Hejtmancik JF, Riazuddin S. Autosomal recessive congenital cataract linked to EPHA2 in a consanguineous Pakistani family. Mol Vis 2010; 16:511-7. [PMID: 20361013].

30. Zhai Y, Zhu S, Li J, Yao K. A novel human congenital cataract mutation in EPHA2 kinase domain (p.G668D) alters receptor stability and function. Invest Ophthalmol Vis Sci 2019; 60:4717-26. [PMID: 31725171].

Articles are provided courtesy of Emory University and the Zhongshan Ophthalmic Center, Sun Yat-sen University, P.R. China. The print version of this article was created on 1 July 2021. This reflects all typographical corrections and errata to the article through that date. Details of any changes may be found in the online version of the article.